Preparation, characterization, and assessment of the antiglioma effects of liposomal celastrol

Yulun Huang[a,d], Dai Zhou[a], Taijun Hang[b], Zhenghong Wu[c], Jiangang Liu[a], Qinan Xu[a], Xuesun Xie[a], Jianling Zuo[a], Zhong Wang[a] and Youxin Zhou[a]

The role of celastrol in the treatment of cancer has been an area of growing interest. To circumvent the issues of low solubility, poor bioavailability, and systemic toxicity of celastrol, we prepared liposomal celastrol using the thin-film dispersion method. We characterized particle size, encapsulation efficiency, and pharmacological parameters of liposomal celastrol. The drug concentration in plasma and tissues was measured using LC-MS/MS. In addition, the sulforhodamine B assay was used to determine the 50% inhibiting concentration. We assessed the effects of the compound in SHG-44 glioma subcutaneous xenografts in BALB/c nude mice. To compare the toxic effects of liposomal and free celastrol, the weight as well as hematologic, heart, liver, and kidney parameters were measured weekly and the morphology of organ tissues was observed pathologically. We found that liposomal celastrol had high encapsulation efficiency (71.67%) and liposomal celastrol had a higher C_{max} and area under the curve, longer $t_{1/2}$, and better biodistribution than free celastrol. A cytotoxicity assay indicated that free celastrol had lower 50% inhibiting concentration values than the liposomal celastrol; however, treatment of subcutaneous xenografts with 1 mg/kg of liposomal celastrol induced greater antitumor activity than free celastrol at an equimolar concentration. In addition, a 4 mg/kg dose of liposomal celastrol had fewer severe side effects than free celastrol at the same dose. In this study, we found that the use of liposomes as a carrier of celastrol increased the bioavailability and reduced the side effects of the compound. Our findings suggest that liposomal celastrol should be further investigated in the clinical setting. *Anti-Cancer Drugs* **23:515–524** © **2012 Wolters Kluwer Health | Lippincott Williams & Wilkins.**

Anti-Cancer Drugs 2012, **23**:515–524

Keywords: animal xenografts model, celastrol, encapsulation efficiency, glioma, liposomal, pharmacokinetics, side effect, tissue distribution

[a]Department of Neurosurgery, First Affiliated Hospital of Soochow University, Suzhou, [b]Department of Pharmaceutical Analysis, China Pharmaceutical University, [c]School of Pharmacy, China Pharmaceutical University, Nanjing, China and [d]Laboratory of Molecular Neuro-oncology, Texas Children's Hospital, Baylor College of Medicine, Houston, Texas, USA

Correspondence to Youxin Zhou, MD, Department of Neurosurgery, First Affiliated Hospital of Soochow University, 188 Shizi Street, Suzhou 215006, Jiangsu Province, China
Tel: +86 013 915 522 828; fax: +86 051 267 781 170;
e-mail: zhouyxyq2008@sohu.com

Received 2 November 2011 **Revised form accepted** 11 January 2012

Introduction

Celastrol is a natural biologically active compound extracted from the Chinese medicine herb *Tripterygium wilfordii* Hook. It has attracted interest for its potential anti-inflammatory and antitumor effects and has been reported to have in-vitro and in-vivo therapeutic efficacy against various cancer types, including prostate [1], melanoma [2], breast [3], pancreatic [4], non-small-cell lung cancer [5], and glioma [6]. Celastrol can also reduce metastatic tumor burden in mesenterium [7], bone [8], and lung metastatic nodules [9]. Therefore, it is an interesting developmental candidate as a novel chemotherapeutic cancer agent. However, no systematic clinical trials in humans have been conducted with celastrol to date.

The free form of celastrol is only soluble in dimethyl sulfoxide (DMSO) or ethanol. The poor solubility in water makes intravenous and intramuscular administration rather difficult. For all in-vivo cancer models assessed with celastrol, an intraperitoneal injection was used as the route of administration. Celastrol is limited in its clinical utility because of poor bioavailability as well as the occurrence of some side effects, such as weight loss (Y. Huang and Y. Zhou, unpublished observation). To circumvent these limitations, alternative drug delivery vehicles for the administration of celastrol are needed.

Liposomes are lipid bilayer vesicles formed by phospholipids dispersed in water and have the ability to encapsulate both hydrophilic and hydrophobic molecules [10]. As celastrol is hydrophobic, it is considered to be a good candidate for liposome incorporation, as it can be encapsulated in the lipid layer of the liposomes. The encapsulation of drugs into liposomes alters their pharmacokinetics and biodistribution, resulting in an increase in therapeutic efficacy and a decrease in toxicity [11].

The aims of this study were to develop a type of liposomal celastrol and evaluate the pharmacokinetics and tissue distribution of the compound. In addition, we wished to determine whether incorporating celastrol in liposomes could enhance the antitumor effects and reduce the side effects compared with free drug.

All supplementary digital content is available directly from the corresponding author.

0959-4973 © 2012 Wolters Kluwer Health | Lippincott Williams & Wilkins DOI: 10.1097/CAD.0b013e3283514b68

Materials and methods

Materials

Celastrol was purchased from Paypaytech Co. (Purity > 99.3%; Shenzhen, China); soybean phosphatidylcholine (SPC) was purchased from Dongshang Co. (Purity > 90%; Shanghai, China); sodium deoxycholate was purchased from Sigma Co. (St Louis, Missouri, USA); methanol was of chromatographic grade and purchased from Yu Wang Co. (Shandong, China); chloroform was of super grade and purchased from Jiangsu Hanbang Co. (Nanjing, China); polydextran gel Sephadex G-50 was purchased from Pharmacia Biotech (Uppsala, Sweden); absolute methanol was of chromatographic grade and purchased from Merck Co. (Victoria, Australia); ciclesonide was used as an internal standard (IS) and was obtained from the National Institute for the Control of Pharmaceutical and Biological Products(Beijing, China). Other reagents used were analytical grade. Kunming (KM) mice (8–10 weeks old) were obtained from the Experimental Animal Center of Suzhou University (Suzhou, China).

Preparation of liposomes

Liposomes were prepared using the thin-film hydration method previously described [12]. On the basis of this method, 2 mg celastrol, 60 mg SPC, and 4 mg sodium deoxycholate were dissolved in 15 ml chloroform/methanol (2 : 1, v/v). The solution was evaporated under vacuum to remove the solvent at 30°C and 100 rpm. This process yielded a lipid film on the wall of the round-bottom flask and was then placed in a vacuum dryer overnight. The next day, 10 ml of phosphate buffer (pH 7.4) was added to the flask for hydration. After 2 h of incubation at 37°C for hydration, the membranes of the liposomes were resuspended and then sonicated (JY92; Xinzhi Co., Ningbo, China) in an ice bath 60 times using a 2 s pulse with a 3 s interval between pulses. The solution was then filtered through a 0.45 μm polycarbonate membrane filter.

Particle size measurement

Particle size and distribution measurements were conducted using a Malvern Instruments Zetasizer 3000HS laser diffraction grain size analyzer (Malvern, UK). All measurements were performed in triplicate.

Transmission electron microscopic studies

The morphology of the liposomal celastrol was examined by transmission electron microscopy (TEM). Briefly, the liposomal celastrol was sonicated for 30 s. A drop of this suspension was placed on a copper TEM grid and allowed to air dry. The samples were imaged using a Tecnai G220 transmission electron microscope (FEI Co., Hillsboro, Oregon, USA) at 120 keV.

Determination of the encapsulation efficiency

The Sephadex column chromatography method (Sephadex G-50) was used to separate free celastrol from drug-loaded liposomes. After the separation, the encapsulation efficiency (EE) was determined by high-performance liquid chromatography (HPLC) analysis with a Shimadzu HPLC system (LC-10A; Shimadzu Co., Japan) using a Hypersil ODS chromatographic column (200 mm × 4.6 mm, 5 μm; Thermo Scientific Inc., Waltham, Massachusetts, USA) with the wavelength set to 425 nm. The mobile phase consisted of methanol : 1% acetic acid (90 : 10, v/v) at a flow rate of 1.0 ml/min. The celastrol EE was calculated using the following equation: EE (%) = (total amount of celastrol – free celastrol)/total amount of celastrol × 100%.

LC-MS/MS analysis of plasma and tissues

The analysis of samples obtained from KM mice was performed using LC-MS/MS. A Thermo Finnigan TSQ Quantum Ultra AM tandem mass spectrometer equipped with an electrospray ionization source (San Jose, California, USA), a Finnigan surveyor LC pump, and an autosampler were used for the LC–MS/MS analysis. Data acquisition was performed using Xcalibur 1.2 software (Thermo Finnigan). The separation of celastrol and the IS ciclesonide was achieved by an automated injection of 20 μl samples into a reverse-phase C18 analytical column (Hedera ODS-2 4.6 mm × 150 mm, 5 μm) under isocratic conditions that included methanol and water with 0.1% formic acid using the following gradient elution: 0 min (70% methanol) → 8 min (100% methanol) at a flow rate of 1.0 ml/min. All analyses were carried out in positive electrospray ionization with the spray voltage set at 5 kV. The heated capillary temperature was set at 350°C. Nitrogen sheath and auxiliary gas were set at 37 and 5.0 psi, respectively. The argon gas collision-induced dissociation was used with a pressure of 1.0 mTorr. The collision energies were set at 30 eV for celastrol and 18 eV for the IS. The ion transitions chosen for selected reaction monitoring (SRM) were m/z 451.3 → 201.1 for celastrol (Fig. S1A) and m/z 541.1 → 523.1 for the IS (ciclesonide), respectively (Fig. S1B). Biological samples were quantified using the ratio of peak area of celastrol to that of the IS.

Pharmacokinetic studies and biodistribution study

Plasma pharmacokinetic analysis was performed in normal KM mice. All animal experimental protocols were approved by the Institutional Animal Care and Use Committee of Suzhou University and complied with the code of ethics for animal experiments. Sixty KM mice weighing 18–22 g were divided into 10 groups ($n = 6$ for each group). Five groups were administered 4 mg/kg celastrol dissolved in 0.1% DMSO in physiological saline by an intraperitoneal injection. The other five groups were administered 4 mg/kg liposomal celastrol by an intraperitoneal injection. In each treatment group, the mice were sacrificed at 10, 30, 60, 120, and 240 min after drug administration. Blood samples were collected at the time of sacrifice and the brain, kidney, heart, lung, and liver were

removed. Each specimen was rinsed with saline, dried, and weighed.

Tissue and plasma samples were carefully excised. Each tissue sample was precisely weighed and mixed at a 1 : 5 (w/v) ratio with sterile saline and then homogenized. The IS working solution (5.0 μg/ml) was then added to 0.1 ml of plasma samples or 0.5 ml of tissue samples (20 μl for plasma samples and 50 μl for tissue samples, respectively) and the tubes were vortex-mixed for 30 s. After mixing, 5 ml of acetic ether was added and then vortex-mixed again for 3 min. The samples were then centrifuged at 3500 rpm for 10 min and 4 ml of the organic layer was transferred into another tube and evaporated to dryness at 40°C under a gentle stream of nitrogen. The residue was reconstituted with 0.1 ml of the mobile phase by vortex mixing for 1 min. The supernatant obtained after centrifugation at 16 000 rpm for 10 min was transferred to an autosampler vial, and 20 μl of this was injected into the LC-MS/MS system. A peak area ratio (R_x) was calculated from the celastrol and IS chromatographic peak areas. The concentration of celastrol in the plasma or tissues was calculated using the formula $R_x/R_r = C_x/C_r$, where C_x is the concentration of celastrol in the plasma or tissues, C_r the concentration of the sample, and R_r the peak area ratio of the sample. Pharmacokinetic parameters were determined using the software Drug and Statistics (DAS, ver. 2.0; Mathematical Pharmacology Professional Committee of China, Beijing, China).

In-vitro anticancer activity evaluation

Glioma cell culture

The U251 human glioma and murine C6 glioma cell lines were purchased from the Type Culture Collection of the Chinese Academy of Sciences (Shanghai, China). The human glioma cell line SHG44 was established by our laboratory in 1984 and has been widely used in China. Cells were cultured in Dulbecco's modified Eagle's medium supplemented with 10% fetal bovine serum, 100 IU/ml penicillin, and 100 μg/ml streptomycin. The cells were cultured at 37°C in a humidified atmosphere containing 5% carbon dioxide.

Cytotoxicity

Cell growth inhibition was assessed by the sulforhodamine B (SRB) staining assay as previously described [13]. Briefly, the glioma cell lines (U251, SHG44, and C6) were seeded at a density of 5000 cells per well in 96-well plates. The next day, the cells were treated with different concentrations (0.037, 0.111, 0.333, 1, 3, 9, and 27 μg/ml) of either free celastrol dissolved in DMSO or the equivalent concentration of liposomal celastrol. The concentration of DMSO was maintained below 0.1% (w/v) to ensure that it did not have a significant effect on cell proliferation. Cells incubated in Dulbecco's modified Eagle's medium alone were used as blank controls. The cells were incubated for 48 h after treatment. After incubation, the media in the wells were removed and all wells were fixed by adding 200 μl of cold 10% (w/v) TCA at 4°C for 1 h. After removal of TCA, the wells were washed five times with deionized water and then dried. A volume of 100 μl 0.4% (w/v) SRB solution was added to each well and stained at room temperature for 20 min. The wells were then washed five times with 1% acetic acid to remove uncoupled SRB and dried. A volume of 200 μl Tris buffer (10 mmol/l) was added to each well. The plates were gently shaken on an oscillator for 30 min to dissolve the SRB. Finally, the absorbance of each well was read on a microplate reader (BIO-RAD model 680; Bio-Rad Laboratories Inc., Shanghai, China) at a wavelength of 540 nm. The survival rates were calculated using the following formula: survival % = [(A_{540} of the treated cells)/(A_{540} of the blank control cells)] × 100, where A_{540} is the absorbance value. The 50% inhibiting concentration (IC_{50}) was calculated for all samples using SPSS software (version 13.0; IBM Inc., Armonk, New York, USA).

In-vivo anticancer experiments

For the in-vivo xenograft model, 4-week-old adult female BALB/c mice weighing approximately 20 g were subjected to subcutaneous implantations of 5×10^6 SHG44 cells [14]. Starting on the 15th day postimplantation, 36 mice were divided into the following six groups ($n = 6$ for each group): blank liposomes (negative control), cisplatin (2 mg/kg/day, positive control), liposomal celastrol (1 and 4 mg/kg/day), and free celastrol (1 and 4 mg/kg/day). All groups were administered the appropriate treatment by an intraperitoneal injection 5 days per week for 4 weeks. Tumor diameters were measured every day, and tumor volumes were calculated as $(\text{width})^2 \times (\text{length})/2$. After 4 weeks, the mice were sacrificed 2 h after the last treatment and the tumors were excised and rapidly frozen in liquid nitrogen. Tumors were fixed in 10% formalin and embedded in paraffin wax. After fixation, the tumors were sectioned at 4 μm thickness.

Evaluation of side effects related to celastrol

Mice were monitored daily for survival and general health. Animal weights were determined weekly. Whole blood was directly taken from the heart using a heparinized syringe immediately after the animals were euthanatized. Erythrocytes, leukocyte hemoglobin, and platelet numbers were assayed from the whole blood. To assess hepatic function, renal function, and myocardial zymogram, the alanine aminotransferase), aspartate aminotransferase, total protein, albumin, creatinine, blood urea nitrogen, lactate dehydrogenase, creatine kinase, and hydroxybutyrate dehydrogenase were assayed using an automatic biochemistry analyzer. The liver, kidney, lung, heart, and brain from the animals were dissected and fixed in 10% formalin for 48 h and embedded in paraffin. Five-micrometer sections were stained with hematoxylin and eosin and assessed under a light microscope.

Statistical analysis

All data were expressed as average ± SD. A paired *t*-test was used to compare two groups. One-way analysis of variance was used to compare the difference between multiple groups. SPSS v13.0 software was used for statistical analysis. Differences were considered to be statistically significant if *P*-value was less than 0.05.

Results

Preparation and characterization of liposomes

Liposomal celastrol consisted of a homogeneous, semitransparent, colloid solution. The average diameter of the liposomes was 128.1 ± 39.5 nm ($n = 3$). TEM showed that the liposomes were spherical and had smooth surfaces (Fig. 1). The liposomes and free drug separated well with the Sephadex column chromatography method. The liposomes were collected in the 8–20 ml fraction and free drug was collected in the 28–60 ml fraction, which showed a clear separation (Fig. 2). An HPLC analysis calibration curve of celastrol was created by plotting the absorbance (Fig. 3). The EE of celastrol was found to be $71.67 \pm 2.32\%$ ($n = 3$).

Pharmacokinetics

Figure 4 and Table 1 show the plasma concentration, time curves, and pharmacokinetic parameters for liposomal and free celastrol. After administration of liposomal celastrol, the plasma celastrol concentration slowly increased over time and reached the highest peak of 497.3 ng/ml during the initial phase, which was a 59.5% increase compared with free celastrol. The concentration also remained high during the terminal phase. Pharmacokinetics parameters were calculated according to a noncompartmental model. The C_{max}, $AUC_{0-\tau}$ and $AUC_{0-\infty}$ of liposomal celastrol were significantly higher than those for free celastrol ($P < 0.05$), and the T_{max}, $t_{1/2}$, and MRT also exhibited a marked prolongation ($P < 0.05$).

Tissue distribution

The liposomes provided a prolonged and steady level of celastrol in the kidney, lung, heart, and brain after intraperitoneal administration of 4 mg/kg liposomal celastrol (Fig. 5). The $AUC_{0-\infty}$ values in the lung, brain, and heart after liposomal celastrol administration were 3.54-, 2.79-, and 2.66-fold higher than those of free celastrol, respectively ($P < 0.01$). The $AUC_{0-\infty}$ for other tissues was not significantly different in mice given liposomal celastrol or free celastrol ($P > 0.05$) (Table 2).

Cytotoxicity assay

Treatment of all cell lines with celastrol induced a dose-dependent antiproliferative effect for both formulations (Fig. S2). The IC_{50} values of liposomal and free celastrol for the three cell lines tested are shown in Table 3. The results indicated that liposomal celastrol had higher IC_{50} values than free celastrol in glioma cells after 48 h of treatment.

Fig. 1

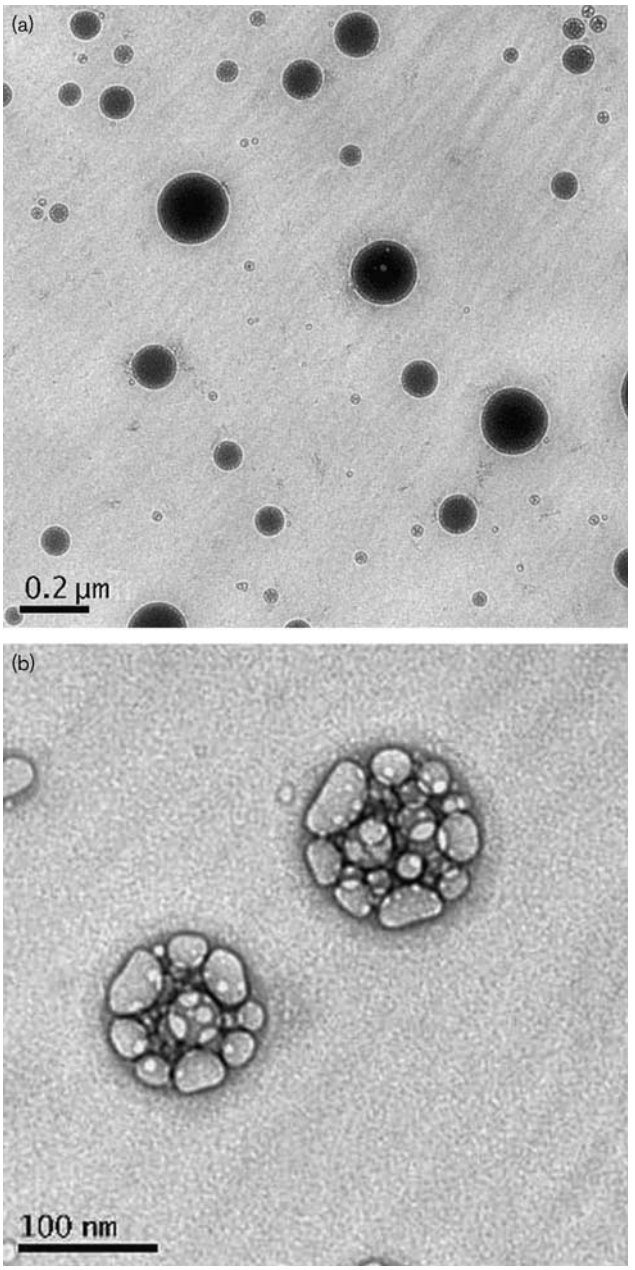

Transmission electron microscopic scan of liposomal celastrol. (a) Low magnification and (b) high magnification.

In-vivo antitumor activity

To test whether liposomal celastrol could enhance the inhibition of human glioma growth, we examined the effects of different celastrol formulations on the growth of human glioma xenografts in nude mice using cisplatin treatment as a positive control. As shown in Fig. 6, the growth of human glioma xenografts was slower in mice treated with liposomal celastrol (1 and 4 mg/kg), free celastrol (4 mg/kg), and cisplatin (2 mg/kg) compared with the blank liposome control. Treatment with 1 mg/kg

Fig. 2

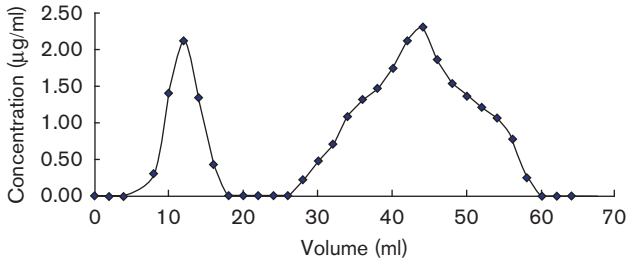

Elution curve of liposomal celastrol and free celastrol. Liposomes were collected in the 8–20 ml fractions and free drug was collected in the 28–60 ml fractions.

Fig. 3

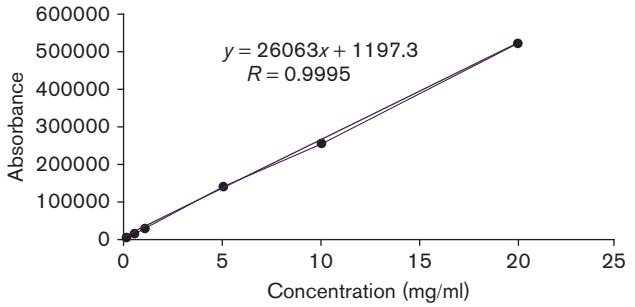

High-performance liquid chromatography (HPLC) calibration curve. An HPLC analysis calibration curve of celastrol was created by plotting the absorbance vs. the concentration.

Fig. 4

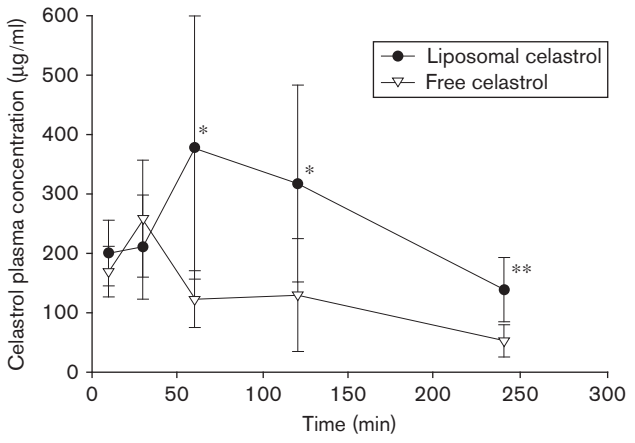

Time course of celastrol levels in plasma from Kunming mice. The celastrol concentration was plotted as a function of time (min) after an intraperitoneal injection of 4 mg/kg liposomal and free celastrol ($n=6$). $^{*}P<0.05$, $^{**}P<0.01$ vs. free celastrol.

liposomal celastrol induced a significantly greater inhibition of tumor growth than 1 mg/kg of free celastrol (32.8 vs. 18.1%, respectively; $P < 0.05$). However, no significant difference was observed between these two treatments at the 4 mg/kg dose (68.4 vs. 66.5%, respectively; $P > 0.05$).

Assessment of side effects

The mice from the free celastrol (4 mg/kg) and cisplatin groups steadily lost weight between days 7 and 28, whereas the liposomal celastrol-treated groups (1 and 4 mg/kg) only experienced a slight variation in weight by day 28 (Fig. 7). The blood analysis of mice from the free celastrol (4 mg/kg) and liposomal celastrol (4 mg/kg) groups showed an increase in leukocyte number compared with the control group, whereas the cisplatin group showed an increase in erythrocyte and hemoglobin values. All other parameters were normal in all groups (data not shown). Only the cisplatin group showed higher blood urea nitrogen values in the renal, hepatic, and myocardial zymogram assessments (data not shown).

In mice treated with free celastrol, the hematoxylin and eosin histopathology examination showed lymphocyte infiltration in liver sinuses, which suggested hepatic prophase injury and slight congestion of renal tubules in the kidney (Figs 8 and 9). The kidney histopathology analysis showed swelling of the renal tubular cells in mice from the cisplatin group, which indicated partial hydropic degeneration. Importantly, none of the groups showed any abnormalities in the lung, heart, or brain.

Discussion

Plant-derived compounds are historically some of the most effective medicines commonly used for therapeutic purposes. Several contemporary, evidence-based therapies are plant derived, including chemotherapeutic drugs, such as paclitaxel and vinca alkaloids. Celastrol is an active ingredient that was originally identified from the traditional Chinese medicine plant *T. wilfordii* Hook almost three decades ago and is generally used for the treatment of inflammatory and autoimmune diseases. Celastrol has attracted great interest recently, especially for its potential antitumor effects. This triterpene has also been found to inhibit the proliferation of a variety of tumor cell lines *in vitro* and inhibit tumor growth in various cancer models *in vivo* [3,6,15–17]. Accumulating experimental evidence suggests that celastrol interferes with a variety of molecular targets, such as the proteasome, heat shock protein 90 (hsp90), nuclear factor-κB, and vascular endothelial growth factor receptor, which are involved in cancer development, progression, and angiogenesis [1,6,18,19]. Importantly, the inhibition of these pathways can lead to the inhibition of cancer cell growth.

The highly hydrophobic nature of celastrol makes intravenous dosing or systemic administration impossible; however, effective methods for the delivery of chemotherapeutics to tumors have recently appeared in the literature. Nanotechnology-based tools and techniques are rapidly emerging in the fields of targeted drug

Table 1 Mean pharmacokinetic parameters of liposomal celastrol and free celastrol after administration to mice

	C_{max} (ng/ml)	T_{max} (h)	$t_{1/2}$ (h)	MRT (h)	$AUC_{0-\tau}$ (μg h/l)	$AUC_{0-\infty}$ (μg h/l)
Liposomal celastrol	497.3 ± 94.4*	1.5 ± 0.6*	7.4 ± 4.8*	9.6 ± 6.3*	1046 ± 140**	2718 ± 1510*
Free celastrol	311.8 ± 136.3	0.4 ± 0.2	2.4 ± 0.8	3.3 ± 0.9	505 ± 216	729 ± 395

$n = 6$; mean ± SD.
AUC, area under the curve.
*$P < 0.05$, **$P < 0.01$.

Fig. 5

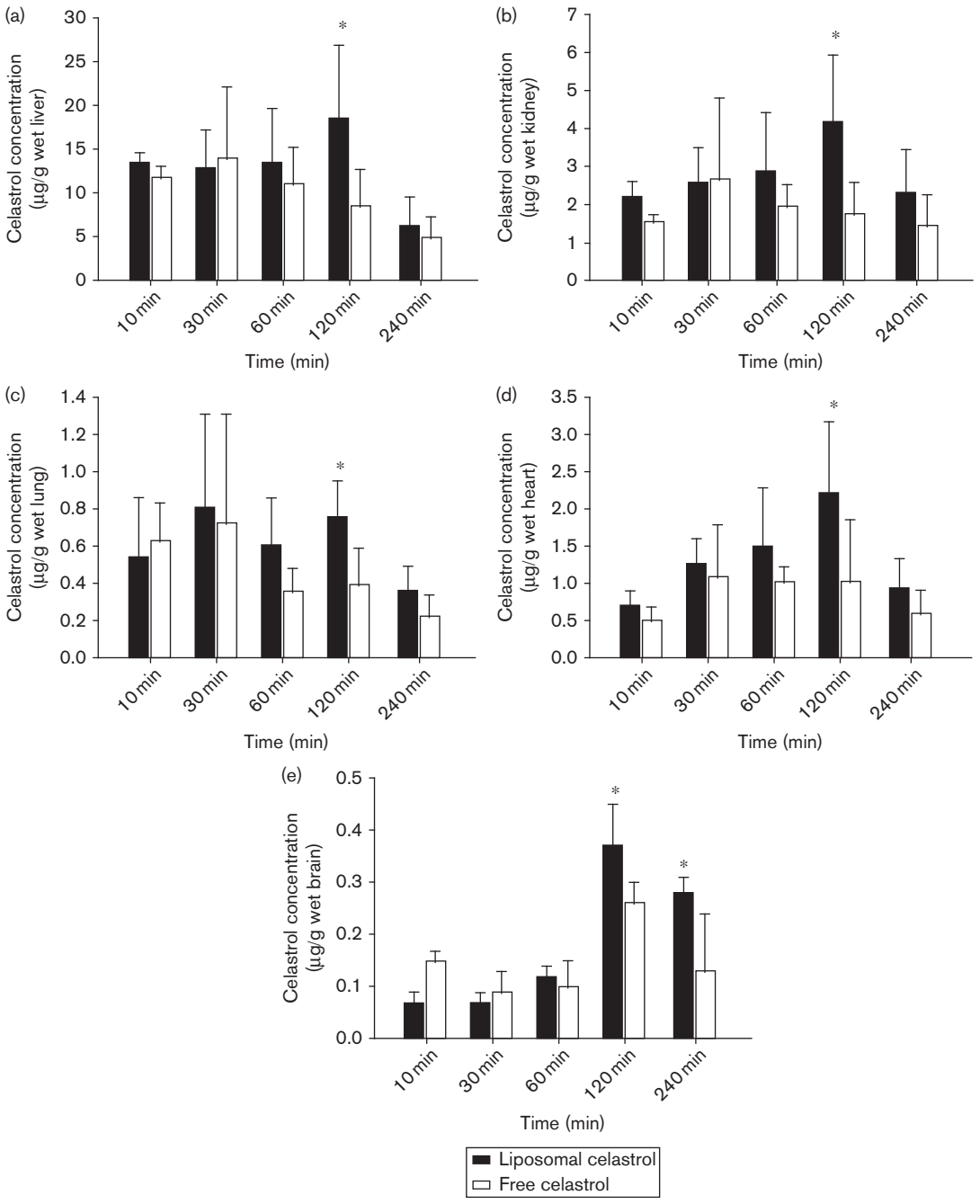

Biodistribution of celastrol in mice. Celastrol concentration was determined in the (a) liver, (b) kidney, (c) lung, (d) heart, and (e) brain tissue of Kunming mice after an injection of liposomal and free celastrol. *$P < 0.05$ vs. free celastrol.

Table 2 Area under tissue concentration time curve after an intraperitoneal injection in mice

	$AUC_{0-\infty}$ of liposomal celastrol (ng h/g)	$AUC_{0-\infty}$ of free celastrol (ng h/g)	Ratio of AUC liposomal/free celastrol
Liver	4950 ± 1882	2975 ± 1165	1.66
Kidney	2182 ± 1004	1253 ± 550	1.74
Lung	496 ± 148**	140 ± 70	3.54
Heart	1111 ± 201**	417 ± 228	2.66
Brain	243 ± 75**	87 ± 27	2.79

$n=6$; mean ± SD.
AUC, area under the curve.
**$P<0.01$ vs. free celastrol.

Table 3 50% inhibiting concentration values of liposomal celastrol and free celastrol in three glioma cells as observed in the cytotoxicity assay

IC_{50} (μg/ml)	SHG44	U251	C6
Free celastrol	0.30 ± 0.06	5.62 ± 0.54	0.69 ± 0.21
Liposomal celastrol	0.89 ± 0.34*	5.70 ± 0.86	3.55 ± 0.92*

$n=3$; mean ± SD.
AUC, area under the curve; IC_{50}, 50% inhibiting concentration.
*$P<0.05$ vs. free celastrol.

Fig. 6

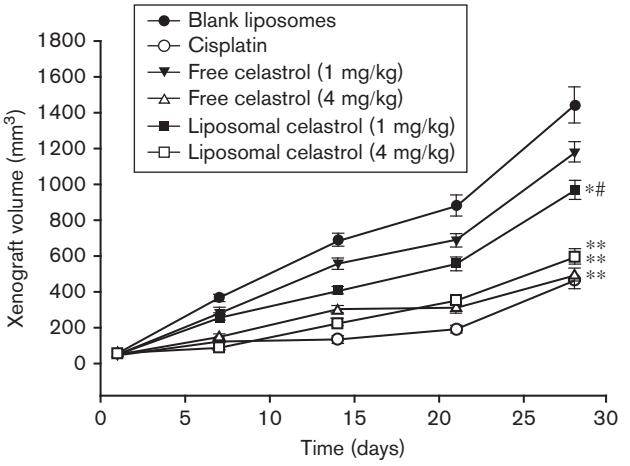

The effects of liposomal and free celastrol on tumor growth *in vivo*. On the 15th day postimplantation, 36 mice were divided into the following six groups ($n=6$ for each group): blank liposomes (negative control), cisplatin (2 mg/kg/day, positive control), liposomal celastrol (1 and 4 mg/kg/day), and free celastrol (1 and 4 mg/kg/day). All groups were administered the appropriate treatment by intraperitoneal injection 5 days per week for 4 weeks. *$P<0.05$, **$P<0.01$ vs. free celastrol; #$P<0.05$ vs. free celastrol (1 mg/kg).

Fig. 7

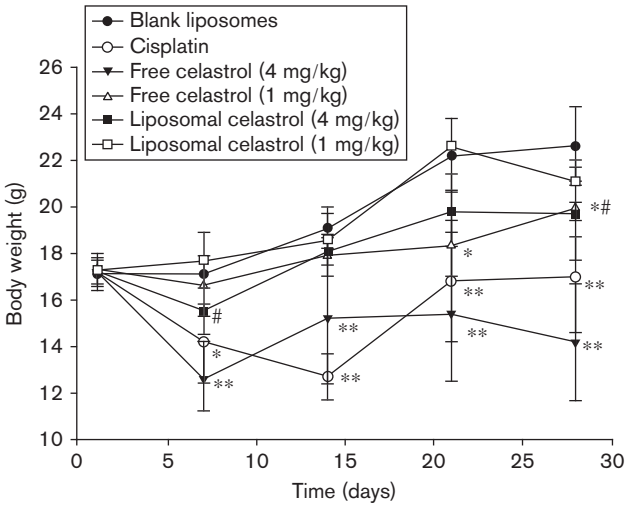

The body weight change in mice administered different treatment options. The mice from the free celastrol (4 mg/kg) and cisplatin groups steadily lost weight between days 7 and 28, whereas the liposomal celastrol-treated groups (4 mg/kg) only experienced a slight variation in weight by day 28. *$P<0.05$, **$P<0.01$ vs. blank liposomal; #$P<0.05$ vs. free celastrol (4 mg/kg).

delivery [20]. Among the various drug delivery vehicles, liposomes have been extensively explored over the past 40 years due to their biodegradability and the potential to load large concentrations of therapeutic agents. Liposomes have the capacity to alter the biodistribution of drugs that they encapsulate through delayed clearance and longer intravascular circulation time. Longer circulation times allow for increased concentration of the liposomal drug in regions of increased vascular permeability, such as solid tumors [21]. The current clinical trials exploring various liposome formulations and the large number of commercially available therapeutics appear promising for the future development of this technology [22]. Liposome entrapment greatly enhances drug accumulation at the tumor site through the enhanced permeability and retention effect. It may also reduce the toxicity of drugs known to have substantial side effects, such as paclitaxel, doxorubicin, and cisplatin. In addition, the liposome has good biocompatibility and does not induce immune system activation or suppression [23].

The thin-film hydration method was first invented by Bangham and colleagues in 1965 [24]. In our study, we developed a new liposomal nanoconstruct composed of celastrol. We used SPC and sodium deoxycholate as the material for the membrane. The EE of this method was 71.67%, and this high efficiency indicated that the liposomal system was well constructed and suitable for large-scale manufacture. The liposome that was created was a large unilamellar vesicle that had a diameter of 128.1 nm. The majority of tumors had a vascular pore cutoff size that ranges between 380 and 780 nm [25]. Therefore, a smaller liposome particle size may be advantageous for passive delivery of the carrier into the tumor interstitium. The accumulation of liposomes in tumor tissue is different from that in normal tissues. Normal tissue contains capillaries with tight junctions that are less permeable to nanosized particles. Scherphof *et al.* [26] demonstrated that the liver sinusoids are permeable to liposomes 100 nm in diameter.

Fig. 8

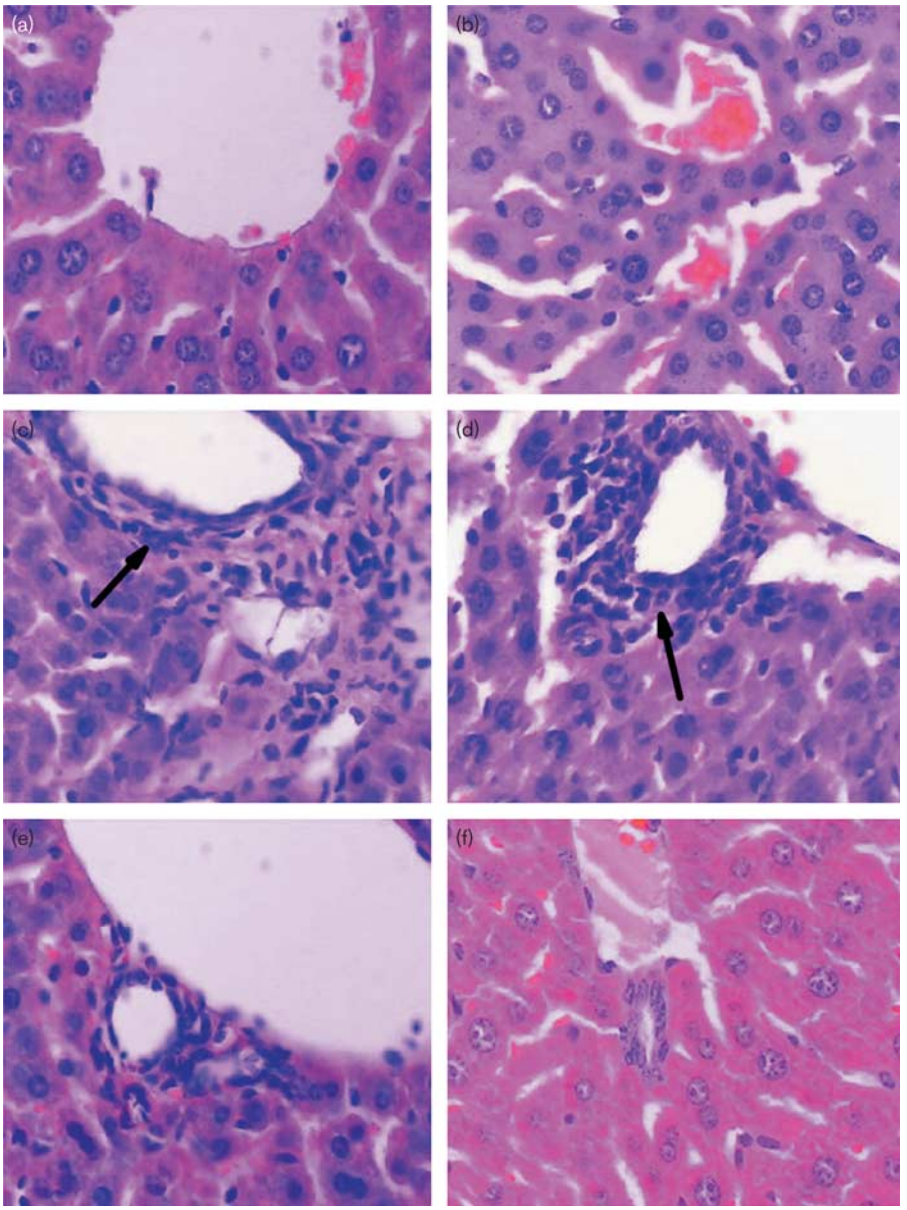

Hepatic histological sections. Histological sections were taken from the following treatment groups and stained with hematoxylin and eosin: (a) blank liposomes, (b) cisplatin, (c) free celastrol (4 mg/kg), (d) free celastrol (1 mg/kg), (e) liposomal celastrol (4 mg/kg), and (f) liposomal celastrol (1 mg/kg). In (c) and (d), arrows indicate lymphocyte infiltration in liver sinuses, which suggested hepatic prophase injury.

To date, a complete pharmacokinetic analysis of celastrol has not been described in the literature. To compare the two formulations, both free and liposomal celastrol were administered to mice by intraperitoneal injection, even though liposomal celastrol can be administered by intravenous injection. When the pharmacokinetics of liposomal and free celastrol were compared, we found that the C_{max} and area under the curve (AUC) of liposomal celastrol in the plasma were increased 1.59- and 3.73-fold compared with free celastrol, and that the MRT and $t_{1/2}$ of liposomal celastrol were prolonged by 2.9- and 3.1-fold, respectively. We hypothesize that the improved pharmacokinetics of liposomal celastrol enhanced the antitumor activity observed *in vivo*. The AUC of liposomal celastrol in the lung, brain, and heart was 3.54-, 2.79-, and 2.66-fold higher than free celastrol, respectively, which were very similar to the ratios observed in the plasma. Therefore, these observations may be attributed to the high plasma concentration and long MRT of liposomal celastrol.

We found that liposomal celastrol had a lower in-vitro IC_{50} than free celastrol in C6, U251, and SHG44 glioma

Fig. 9

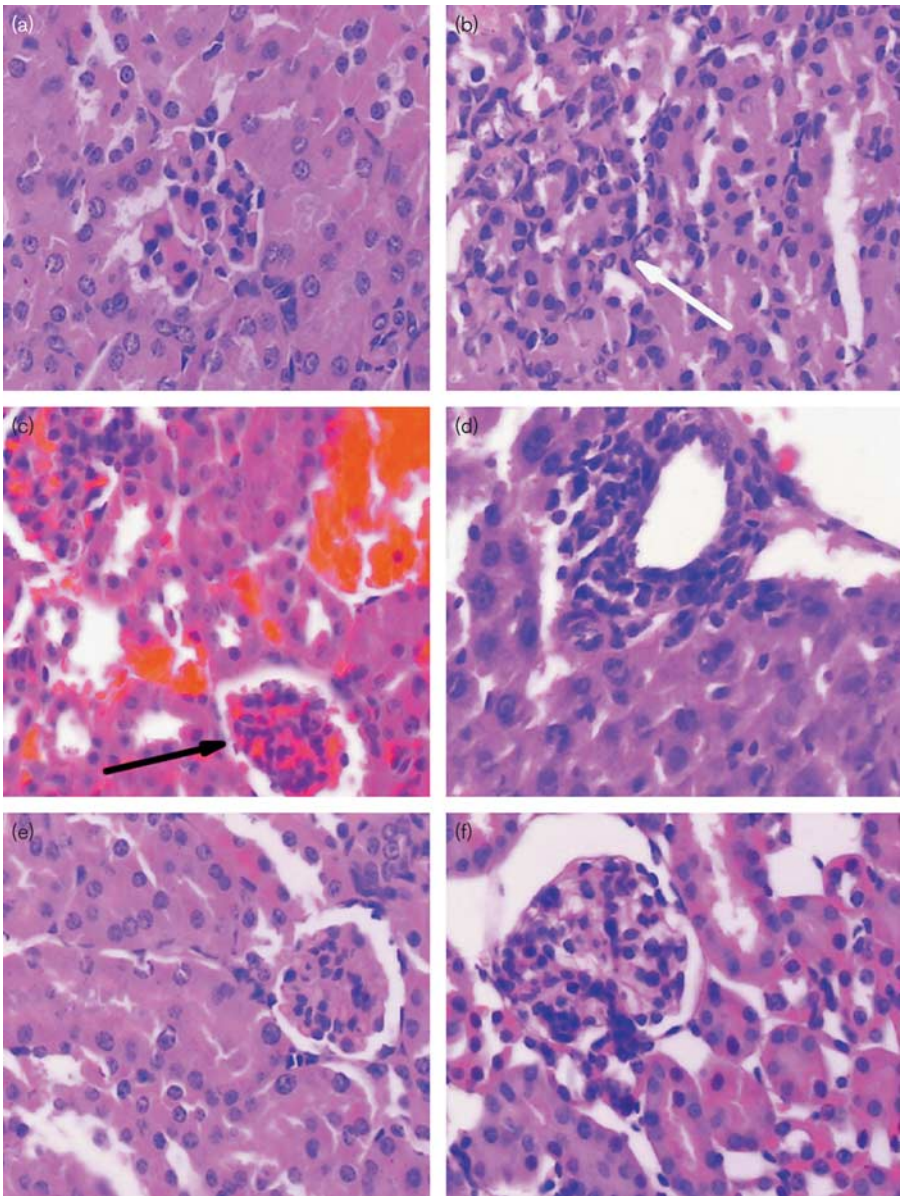

Renal histological sections. Histological sections were taken from the following treatment groups and stained with hematoxylin and eosin: (a) blank liposomes, (b) cisplatin, (c) free celastrol (4 mg/kg), (d) free celastrol (1 mg/kg), (e) liposomal celastrol (4 mg/kg), and (f) liposomal celastrol (1 mg/kg). In (b), the white arrow indicates swelling of the renal tubular cells in mice from the cisplatin group, which indicated partial hydropic degeneration. In (c), the black arrow indicates slight congestion of renal tubules in the kidney.

cell lines. It is possible that free celastrol is directly exposed to glioma cells through passive diffusion and therefore is more easily taken up by glioma cells. In addition, liposomal celastrol may have a reduced uptake rate due to the delay in membrane fusion between the liposome and the cell membrane or a delay in endocytosis [27].

Liposomal celastrol was also found to be active in an in-vivo animal model. The 1 mg/kg dose of liposomal celastrol exhibited greater antitumor activity than free celastrol at equimolar concentrations. However, the 4 mg/kg dose of liposomal celastrol had equivalent antitumor activity *in vivo* as free celastrol at an equimolar concentration, although the side effects were attenuated in the liposomal celastrol group. This type of celastrol administration could also be used for multiple cancer types, such as prostate, breast, and lung cancer.

Because of the blood–brain barrier in the brain, the antiglioma effects of liposomal celastrol will depend on the

ability of the compound to pass through the blood–brain barrier. This characteristic will need to be explored in an intracranial graft model in future studies.

To date, a complete toxicological analysis of celastrol has not been described in the literature. In our study, we found that free celastrol induced some side effects *in vivo*, including weight loss, mild hepatic injury, and slight kidney dysfunction. In contrast, these changes were not observed in the liposomal celastrol group. The body weight of the mice in the free celastrol (4 mg/kg) group decreased 37%, whereas the decrease in weight in mice of the liposomal celastrol group was less than 12.8%. Therefore, liposomalization of celastrol appears to be able to reduce its toxicity. Taken together, our observations suggest that liposomal celastrol should be investigated in the clinical setting.

Conclusion

In this study, we assessed the use of liposomes as a delivery method for celastrol. The results presented here provide strong evidence that liposomes can be effective delivery vehicles of celastrol that increase the antitumor activity and reduce the side effects of the compound.

Acknowledgements

Youxin Zhou is currently receiving Jiangsu Province Outstanding Medical Academic Leader program and Innovation Team Fund (No. K201106) and Suzhou Municipal Development Plans (SYS201025). Zhong Wang is currently receiving Jiangsu Province Outstanding Medical Academic Leader program (No LJ201139).

Conflicts of interest

There are no conflicts of interest.

References

1 Yang H, Chen D, Cui QC, Yuan X, Dou QP. Celastrol, a triterpene extracted from the Chinese ''Thunder of God Vine,'' is a potent proteasome inhibitor and suppresses human prostate cancer growth in nude mice. *Cancer Res* 2006; **66**:4758–4765.
2 Abbas S, Bhoumik A, Dahl R, Vasile S, Krajewski S, Cosford ND, *et al.* Preclinical studies of celastrol and acetyl isogambogic acid in melanoma. *Clin Cancer Res* 2007; **13**:6769–6778.
3 Jang SY, Jang SW, Ko J. Celastrol inhibits the growth of estrogen positive human breast cancer cells through modulation of estrogen receptor alpha. *Cancer Lett* 2011; **300**:57–65.
4 Zhang T, Hamza A, Cao X, Wang B, Yu S, Zhan CG, *et al.* A novel Hsp90 inhibitor to disrupt Hsp90/Cdc37 complex against pancreatic cancer cells. *Mol Cancer Ther* 2008; **7**:162–170.
5 Mou H, Zheng Y, Zhao P, Bao H, Fang W, Xu N. Celastrol induces apoptosis in non-small-cell lung cancer A549 cells through activation of mitochondria- and Fas/FasL-mediated pathways. *Toxicol In Vitro* 2011; **25**:1027–1032.
6 Huang Y, Zhou Y, Fan Y, Zhou D. Celastrol inhibits the growth of human glioma xenografts in nude mice through suppressing VEGFR expression. *Cancer Lett* 2008; **264**:101–106.
7 Zhang T, Li Y, Yu Y, Zou P, Jiang Y, Sun D. Characterization of celastrol to inhibit hsp90 and cdc37 interaction. *J Biol Chem* 2009; **284**: 35381–35389.
8 Idris AI, Libouban H, Nyangoga H, Landao-Bassonga E, Chappard D, Ralston SH. Pharmacologic inhibitors of IkappaB kinase suppress growth and migration of mammary carcinosarcoma cells in vitro and prevent osteolytic bone metastasis in vivo. *Mol Cancer Ther* 2009; **8**: 2339–2347.
9 Zhu H, Liu XW, Cai TY, Cao J, Tu CX, Lu W, *et al.* Celastrol acts as a potent antimetastatic agent targeting beta1 integrin and inhibiting cell-extracellular matrix adhesion, in part via the p38 mitogen-activated protein kinase pathway. *J Pharmacol Exp Ther* 2010; **334**:489–499.
10 Kim S. Liposomes as carriers of cancer chemotherapy. Current status and future prospects. *Drugs* 1993; **46**:618–638.
11 Papahadjopoulos D, Allen TM, Gabizon A, Mayhew E, Matthay K, Huang SK, *et al.* Sterically stabilized liposomes: improvements in pharmacokinetics and antitumor therapeutic efficacy. *Proc Natl Acad Sci USA* 1991; **88**:11460–11464.
12 Ferreira H, Lucio M, Lima JL, Matos C, Reis S. Interaction of clonixin with EPC liposomes used as membrane models. *J Pharm Sci* 2005; **94**:1277–1287.
13 Wang W, Yang S, Su Y, Xiao Z, Wang C, Li X, *et al.* Enhanced antitumor effect of combined triptolide and ionizing radiation. *Clin Cancer Res* 2007; **13**:4891–4899.
14 Ushiro S, Ono M, Nakayama J, Fujiwara T, Komatsu Y, Sugimachi K, *et al.* New nortriterpenoid isolated from anti-rheumatoid arthritic plant, *Tripterygium wilfordii*, modulates tumor growth and neovascularization. *Int J Cancer* 1997; **72**:657–663.
15 Dai Y, Desano J, Tang W, Meng X, Meng Y, Burstein E, *et al.* Natural proteasome inhibitor celastrol suppresses androgen-independent prostate cancer progression by modulating apoptotic proteins and NF-kappaB. *PLoS One* 2010; **5**:e14153.
16 Lee JH, Koo TH, Yoon H, Jung HS, Jin HZ, Lee K, *et al.* Inhibition of NF-kappa B activation through targeting I kappa B kinase by celastrol, a quinone methide triterpenoid. *Biochem Pharmacol* 2006; **72**:1311–1321.
17 Pang X, Yi Z, Zhang J, Lu B, Sung B, Qu W, *et al.* Celastrol suppresses angiogenesis-mediated tumor growth through inhibition of AKT/mammalian target of rapamycin pathway. *Cancer Res* 2010; **70**:1951–1959.
18 Peng B, Xu L, Cao F, Wei T, Yang C, Uzan G, *et al.* HSP90 inhibitor, celastrol, arrests human monocytic leukemia cell U937 at G0/G1 in thiol-containing agents reversible way. *Mol Cancer* 2010; **9**:79.
19 Sethi G, Ahn KS, Pandey MK, Aggarwal BB. Celastrol, a novel triterpene, potentiates TNF-induced apoptosis and suppresses invasion of tumor cells by inhibiting NF-kappaB-regulated gene products and TAK1-mediated NF-kappaB activation. *Blood* 2007; **109**:2727–2735.
20 Caruthers SD, Wickline SA, Lanza GM. Nanotechnological applications in medicine. *Curr Opin Biotechnol* 2007; **18**:26–30.
21 Allen TM. Liposomal drug formulations. Rationale for development and what we can expect for the future. *Drugs* 1998; **56**:747–756.
22 Goyal P, Goyal K, Vijaya Kumar SG, Singh A, Katare OP, Mishra DN. Liposomal drug delivery systems – clinical applications. *Acta Pharm* 2005; **55**:1–25.
23 Metselaar JM, Mastrobattista E, Storm G. Liposomes for intravenous drug targeting: design and applications. *Mini Rev Med Chem* 2002; **2**: 319–329.
24 Bangham AD, Standish MM, Watkins JC. Diffusion of univalent ions across the lamellae of swollen phospholipids. *J Mol Biol* 1965; **13**:238–252.
25 Hobbs SK, Monsky WL, Yuan F, Roberts WG, Griffith L, Torchilin VP, *et al.* Regulation of transport pathways in tumor vessels: role of tumor type and microenvironment. *Proc Natl Acad Sci USA* 1998; **95**:4607–4612.
26 Scherphof GL, Dijkstra J, Spanjer HH, Derksen JT, Roerdink FH. Uptake and intracellular processing of targeted and nontargeted liposomes by rat Kupffer cells in vivo and in vitro. *Ann N Y Acad Sci* 1985; **446**: 368–384.
27 Wrobel I, Collins D. Fusion of cationic liposomes with mammalian cells occurs after endocytosis. *Biochim Biophys Acta* 1995; **1235**: 296–304.